JOURNAL OF SOLID STATE CHEMISTRY 35, 325–333 (1980)

The "Grain-Boundary Effect" in Doped Ceria Solid Electrolytes

DA YU WANG AND A. S. NOWICK

Henry Krumb School of Mines, Columbia University, New York, New York 10027

Received January 14, 1980

The ac electrical behavior of sintered polycrystalline CeO_2 : CaO and CeO_2 : Y_2O_3 solid electrolytes is studied. Complex impedance plots show the presence of an extra arc due to the presence of relatively high-resistivity material along the grain boundaries. This "grain-boundary effect" is greatest for dilute solid solutions and "pure" samples and becomes vanishingly small for dopant concentrations $\gtrsim 15$ mole%. The effect can also be reduced by shortening the sintering time. The activation enthalpy for the grain-boundary conductivity is substantially higher than that of the lattice conductivity, especially at low dopant levels. This fact eliminates the Bauerle constriction model. The results suggest that the effective dopant concentration near the grain boundaries may be substantially reduced from the bulk value.

Introduction

Solid electrolytes that are good oxygen-ion conductors are of particular interest for application in high-temperature fuel cells (*1*). The best materials of this type are the oxides of the fluorite structure, doped with divalent or trivalent cations so as to introduce a relatively high concentration of oxygen-ion vacancies. When a good ionic conductor is placed in a cell, however, its performance may be limited by factors other than its conductivity, e.g., by blocking effects at electrodes or at grain boundaries. In order to separate out such effects ac techniques are very useful, and in particular, complex impedance (or admittance) plots (*2, 3*). In such plots, one ideally expects one or two arcs caused by electrode effects and, at the highest frequencies, a single arc representing the bulk (*4*). In fact, however, for polycrystalline materials, an extra arc is often obtained which is related to a grain-boundary effect. This effect, which is attributable to a high resistance or blocking layer along the grain boundaries, has been most thoroughly studied for doped zirconia electrolytes (*2, 5–7*) but has also been observed in other cases, particularly for β-alumina (*8, 9*) which is an alkali-ion conductor.

In his study of zirconia electrolytes, Bauerle (*2*), using an electron microprobe, found a second phase containing SiO_2 and CaO in the grain-boundary region. When high-purity materials were used and sintering was carried out in a contamination-free furnace, the grain-boundary effect was reduced to a negligible magnitude. Bauerle also observed that the grain-boundary effect involved the same activation energy as the lattice conductivity and concluded that it was a constriction-resistance effect, i.e., that passage of the ionic current was only possible in limited (unblocked) regions of the grain boundary. In later work, Beekmans and Heyne (*5*) showed that the existence of dispersion effects in the con-

0022-4596/80/150325-09$02.00/0

ductivity of zirconia depended on the composition of the second phase at the grain boundaries, and in particular, that the presence of silica was a major factor while alumina did not contribute to the effect. The conclusions are supported by the work of Schouler *et al.* (*6*) who obtained a large effect when they deliberately doped the sample with SiO_2. They also demonstrated aging effects which were interpreted in terms of the precipitation of dissolved silica at grain boundaries.

The present work is carried out on ceria (CeO_2) doped with CaO and Y_2O_3. This material has two advantages over doped zirconia: first, its bulk ionic conductivity is higher (*10*) and second, pure CeO_2 possesses the fluorite structure, so that, unlike stabilized zirconia, it can be studied at very low dopant levels. It will be shown that striking grain-boundary effects are observed, and that the results differ in important ways from those for zirconia.

Experimental Methods

Samples were prepared in the form of sintered pellets by both mechanical and chemical methods. For mechanically prepared samples, mixed powder of the desired composition was first calcined at 1000°C, then ground and pressed into pellets (1.70 cm in diameter × 0.2 cm high), and finally sintered in air at 1500°C for 48 hr. The density thus obtained is greater than 88% of the theoretical value. For chemically prepared samples, mixed powder of the desired composition was first dissolved in nitric acid. Precipitation was then carried out by the addition of ammonium hydroxide. After filtering and drying, the powder was calcined at 1000°C for 12 hr, reground, pressed into pellets, and sintered at 1500°C for 4 days. The density of such chemically prepared samples is usually greater than 90% of the theoretical density.

Two different purities of ceria powder were obtained from Atomergic Chemetals Company. The first (nominally 99.95% pure) will be designated in this paper as "low purity," while the second (nominally 99.999% pure) will be designated "high purity." Analysis is not available. Only the 0.15% yttria-doped samples and some of the pure samples were prepared from this "high-purity" powder; the others were from the "low-purity" material.

Most of the dc conductivity measurements used the four-probe method. Samples were cut into the shape of bars and four platinum-wire electrodes were wrapped around them with the help of a nonflux platinum paste (Engelhard 6926) to improve the contact resistance. The sample chamber was made of quartz and surrounded by a kanthal-wound resistance furnace controlled to within ±1°C.

Unless indicated otherwise, the dc conductivity measurements were carried out in pure oxygen or in open air atmospheres. For some measurements where P_{O_2} dependence was required, CO–CO_2 gas mixtures from the Matheson Gas Company were used. The mixed gases were first passed through a calcia-stabilized zirconia cell to monitor the partial pressure of oxygen, and then fed into the sample chamber (volume ~560 cm^3) at a rate 100–300 cm^3/min.

For ac conductivity measurements, two separate pieces of equipment were utilized, each covering different conductance ranges. The General Radio capacitance bridge assembly (1620A) with a frequency range 50 Hz–10 kHz was used for low-temperature measurements. For high-temperature measurements, a Hewlett-Packard 3575A gain phase meter was used over a frequency range 1 Hz–13 MHz. Details of the measurements employing tis gain phase meter have been given previously (*11*).

Samples for ac measurements were disk-shaped. For electrodes, the surface was brushed with platinum paste (Engelhard 6082) or flexible silver coating (Engelhard

No. 16). Platinum gauze (52 mesh) was placed on top of the electrode which was then connected to platinum-wire electrical leads. Temperature control of the furnace was to within ±1°C.

Results

When the ac measurements were graphed on complex impedance plots (Z'' vs Z', where Z' is the real part and Z'' the negative imaginary part of the complex impedance) three distinct arcs were generally observed. Because of the limited frequency range of the equipment (1 Hz–13 MHz), however, not all of the arcs appear at any one temperature. Figure 1 illustrates this behavior for the case of a 6% Y_2O_3-doped sample.[1] The arcs are numbered from low to high frequency. At the higher temperature arcs 1 and 2 are observed. As the temperature is lowered, arc 1 gradually shifts into the range below 1 Hz, while eventually arc 3 moves into the higher-frequency range of the measurements. The intersection of arcs 1 and 2 on the real axis is denoted by R_{12}, while that of arcs 2 and 3 by R_{23}.

The appearance of three successive semicircular arcs in a complex impedance diagram means that the equivalent circuit of the specimen can be represented as three parallel R–C elements in series with one another, as shown in Fig. 2. Each such element corresponds to one of the observed arcs. From Fig. 2 we see that

$$R_{12} = R_l + R_{gb}, \tag{1}$$

while

$$R_{23} = R_l. \tag{2}$$

The fact that the observed arcs are depressed (i.e., their centers fall below the real axis, with depression angles as marked

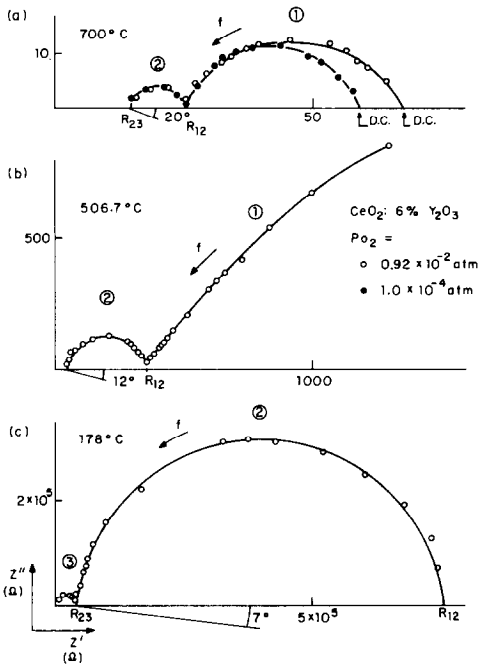

FIG. 1. The ac complex impedance plots (Z'' versus Z') for CeO_2: 6%Y_2O_3 at three different temperatures showing the three arcs. D.C. denotes resistance values obtained by a two-probe measurement. The top figure shows data at two different oxygen partial pressures.

in Fig. 1) shows that this equivalent circuit is not a completely accurate representation, but rather that each arc corresponds to a narrow distribution of R–C elements. For simplicity, we will ignore this discrepancy for the present.

Figure 1a also shows that arc 1 has a strong dependence on the partial pressure of oxygen of the ambient gas. It has been demonstrated elsewhere (*11*) that this arc originates in electrode polarization effects. The fact that the resistance measured by a

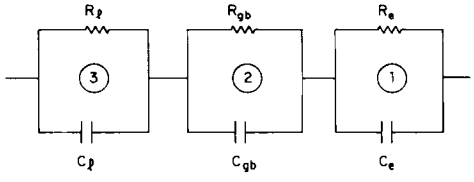

FIG. 2. The equivalent circuit that gives rise to the three arcs of the complex impedance plot.

[1] Throughout this paper % Y_2O_3 or % CaO refers to mole percent.

two-probe dc method (denoted by D.C. on the graph) agrees with the intersection of arc 1 with the Z' axis on the low-frequency side, and that a four-probe dc measurement agrees with the intersection, R_{12}, on the high-frequency side, firmly establishes this conclusion. Thus, arcs 2 and 3 are related to the behavior of the electrolyte itself. The two intersection points R_{12} and R_{23} can be converted into conductivities (σ) by the relation

$$\sigma = d/AR, \tag{3}$$

where d and A are the sample thickness and area, respectively. The results may then be plotted in the usual conductivity plot, log σT vs $1/T$, as shown in Fig. 3. Here the lower curve (solid triangles) is obtained from values R_{12} and the upper curve (open triangles) from R_{23}. In addition, results of four-probe dc measurements are plotted as open circles, and verify the agreement with R_{12} mentioned above. Both curves can be fitted to the conventional equation

$$\sigma T = A \exp(-H/kT), \tag{4}$$

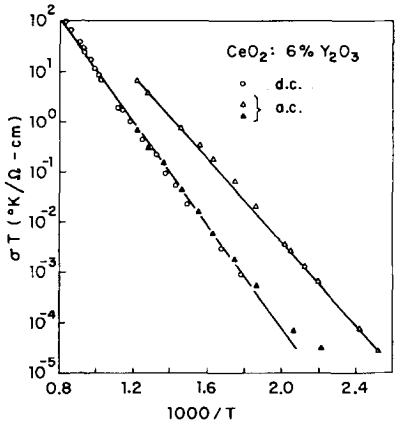

FIG. 3. Plot of σT versus reciprocal absolute temperature for the CeO_2: 6%Y_2O_3 sample. Three sets of data are incorporated: open circles are from four-probe dc measurements, solid triangles are obtained from ac data for R_{12}, and open triangles from ac data for R_{23}.

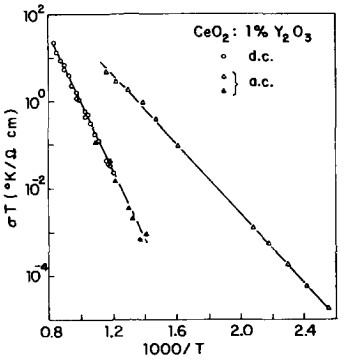

FIG. 4. Plots of σT versus $1/T$ for a CeO: 1%Y_2O_3 sample. Symbols have the same significance as in Fig. 3.

in which H is the activation enthalpy and A the preexponential factor.

Similar plots for the 1 and 15% Y_2O_3 electrolytes are shown in Figs. 4 and 5, respectively. Comparing Figs. 3–5 shows that the separation between the upper and lower conductivity curves is greater the lower the Y_2O_3 content and becomes very

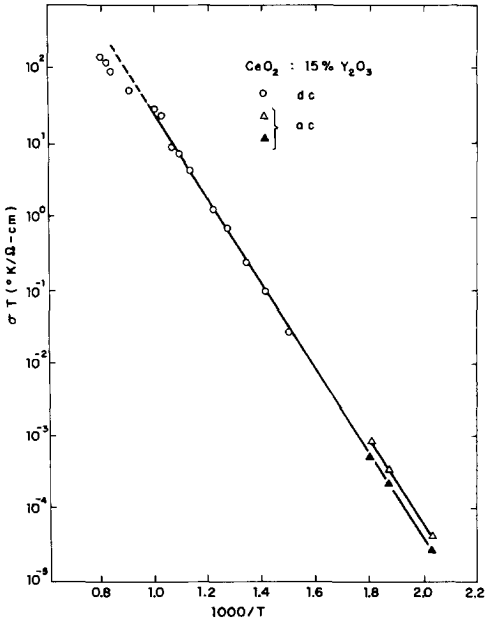

FIG. 5. Plots of σT versus $1/T$ for a CeO_2: 15%Y_2O_3 sample. Symbols have the same significance as in Fig. 3.

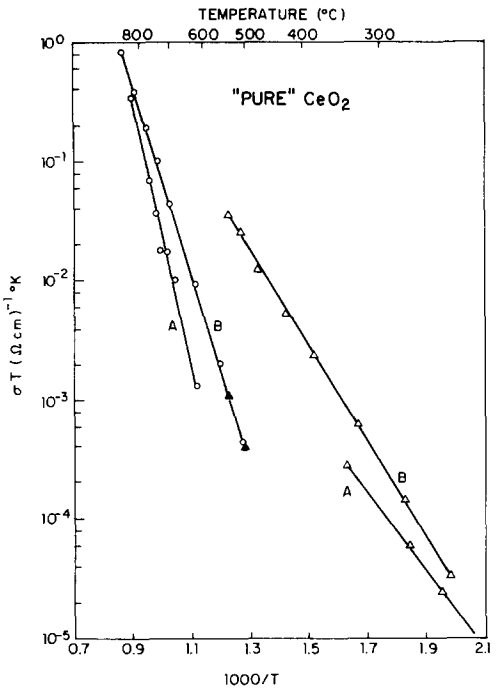

FIG. 6. Plots similar to Fig. 3 for "pure" CeO_2 of both high purity (curves A) and low purity (curves B).

small for 15% Y_2O_3. For the case of a 40% Y_2O_3 sample, arc 2 is not observed at all; therefore only a single R–C element is needed to represent the electrolyte.

In view of this composition dependence of the size of arc 2, it seemed of interest also to examine samples of nominally pure ceria. Results for the high-purity material are shown in Fig. 6 as curves A, and for the low-purity material as curves B. It is clear that the trend of larger separation with increasing purity continues in these "pure" materials.

From the frequency f_m at the peak of Z'' for arcs 2 and 3, the corresponding capacitances C_{gb} and C_l, respectively, may be obtained. It is always found that C_{gb} is in the range of tens of nanofarads, while C_l is in the range of tens of picofarads, i.e. almost 10^3 times smaller. In fact, the values of C_l are consistent with the geometric capacitance of the sample (with a dielectric

TABLE I

VALUES OF CAPACITANCE AND DEPRESSION ANGLES FOR THE GRAIN-BOUNDARY ARC 2 FOR CeO_2: 1% Y_2O_3[a]

Temp. (°C)	C_{gb} (nF)	Depress. angle (°)	f_m (Hz)
788	54	15	200k
746	51	15	90k
706	51	20	40k
643	52	19	13k
595	50	18	4.7k
545	50	16	1.5k
499	50	19	460
448	51	21	95

[a] Sample thickness 0.65 mm, electrode area 1 cm^2, average grain size 8.6 μm).

constant ~50). This suggests that R_{23} (= R_l of Fig. 2) is the lattice resistance and that the upper curves of Figs. 3–6 give, in fact, the lattic conductivity, σ_l. The second arc, and the element R_{gb}–C_{gb} of the equivalent circuit, then represent the effect of a grain boundary layer of higher resistance than the lattice. The corresponding ratio C_{gb}/C_l ~ 10^3 suggests that this layer occupies about 1/1000th of the thickness of the grain.

Tables I and II give a compilation of data for arcs 2 and 3 of the 1% Y_2O_3 sample, showing that the capacitances C_{gb} and C_l,

TABLE II

VALUES OF CAPACITANCE AND DEPRESSION ANGLES FOR THE LATTICE ARC 3 FOR THE SAME SAMPLES AS IN TABLE I

Temp. (°C)	C_l (pF)	Depress. angle (°)	f_m (Hz)
200	73	10.5	60k
179	66	9.5	28k
159.9	62	11	13k
139.3	76	14.5	4k
120.4	73	13	1.5k
99	73	17	400

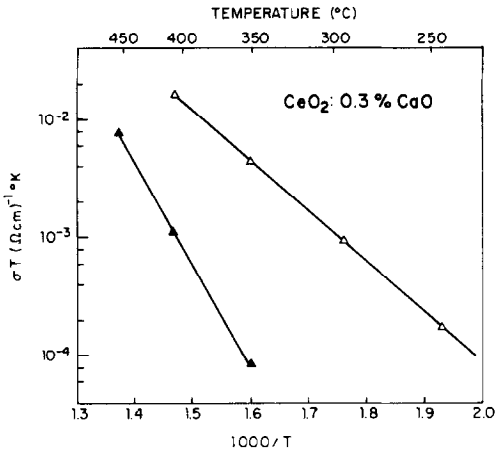

FIG. 7. Plot of σT versus $1/T$ for the CeO_2: 0.3%CaO sample based on ac measurements. Solid triangles are data obtained from R_{12} and open triangles from R_{23}.

as well as the corresponding depression angles, do not vary systematically with the temperature over the present range of measurement.

For calcia-doped ceria the results are less striking than for the yttria-doped samples. Figure 7 shows the results for the 0.3% CaO sample, where the two conductivity curves are well separated; on the other hand, the 1% sample (not shown) only gives a very small separation. The data for the 15% sample, shown in Fig. 8, are interesting in that a crossing of the curves has taken place, such that the high-temperature dc measurements fall on the extrapolation of the ac data for σ_l (the open triangles) rather than those from σ_{12} (the closed triangles). The 1% CaO sample also shows this effect.

In Table III we have collected the conductivity results based on σ_{12} (i.e., the lower curves of plots such as Fig. 3) including the activation enthalpy, preexponential constant A, and the separation, $\Delta \log_{10}\sigma$, between the upper and lower conductivity curves at 350°C ($1000/T = 1.6$), for various "pure," Y_2O_3-doped, and CaO-doped samples. From Eqs. (1) and (3), the lower curve

TABLE III

ACTIVATION ENTHALPY AND PREEXPONENTIAL FACTOR FOR THE LOWER CONDUCTIVITY PLOTS[a] AS WELL AS THE SEPARATION, $\Delta \log \sigma$, BETWEEN THE UPPER AND LOWER PLOTS AT 350°C ($1000/T = 1.6$), FOR VARIOUS "PURE" AND DOPED CERIA SAMPLES

CeO_2 composition	H (eV)	A (°K/Ω-cm)	$\Delta \log \sigma$
High purity	2.2	3.6×10^9	>3
Low purity	1.65	1.7×10^7	3.0
1% Y_2O_3	1.53	3.6×10^7	3.7
6% Y_2O_3	1.01	1.2×10^6	1.3
8% Y_2O_3	0.99	5.2×10^6	0.3
15% Y_2O_3	1.17	7.8×10^7	0.2
0.3% CaO	1.28	1.5×10^6	1.5
1% CaO	0.92	2.6×10^5	0.3

[a] Obtained from σ_{12} and four-probe dc data.

gives $(\sigma_l^{-1} + \sigma_{gb}^{-1})^{-1}$, but when the separation is large, these conductivity results, to a good approximation, represent σ_{gb}, the contribution from the material in the grain-

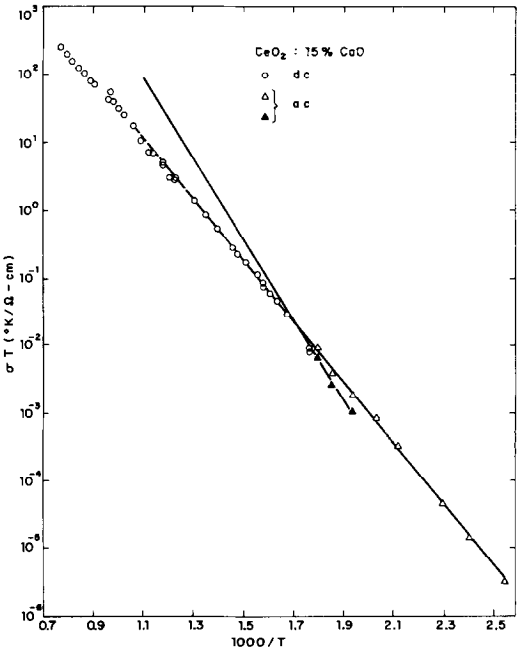

FIG. 8. Plot of σT versus $1/T$ for the CeO_2: 15%CaO sample. Symbols have the same significance as in Fig. 3.

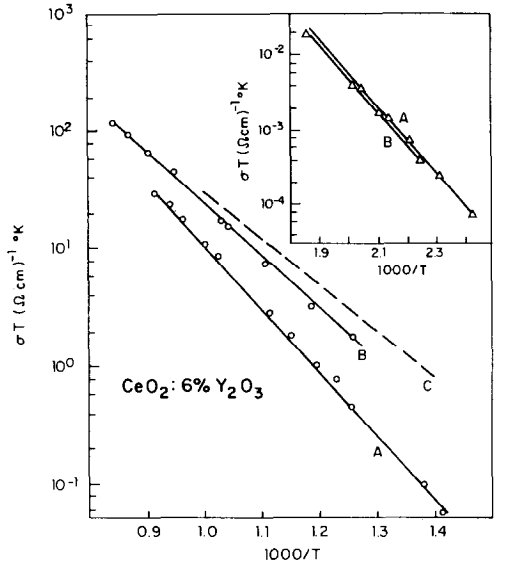

FIG. 9. Effect of sintering time on conductivity of CeO_2: 6%Y_2O_3. Sample A is given the standard (4-day) sintering at 1500°C, while sample B is sintered for only 12 hr. Circles are dc four-probe measurements, and triangles are ac data from R_{23} (i.e., representing σ_l). Curve C is for CeO_2: 5%Y_2O_3 sintered for 12 hr (from Ref. (*10*)).

boundary region. The high activation enthalpy for this grain-boundary conductivity, relative to that for the lattice (~0.8–0.9 eV), is particularly noteworthy for the "pure" and slightly doped samples.

A number of experiments were carried out in order to determine what factors influence the magnitude of the grain-boundary effect, i.e., the separation Δ log σ, or the size of arc 2. Because a chemical preparation method was used for the Y_2O_3-doped samples and a mechanical preparation for the CaO-doped samples, we have compared the results of Fig. 4 with those for a mechanically prepared 1% Y_2O_3 sample for the same sintering. No appreciable difference was found. Also a sample sintered in flowing argon gas was compared with one given the usual sintering in still air; again no appreciable difference was observed.

A factor that did affect the magnitude of the grain-boundary effect was the sintering time. An example is given in Fig. 9 where a 6% Y_2O_3-doped sample sintered for 12 hr at 1500°C (curve B) is compared with one that received the standard 4 days at 1500°C (curve A). Also shown (dashed curve C) are data from Tuller and Nowick (*10*) for a 5% Y_2O_3 sample which also had the short sintering time. All of the data in the main plot are results of four-probe dc measurements. In the inset, the lattice conductivity σ_l of samples A and B at lower temperatures is shown; the slight difference between the two curves is not regarded as significant. It is thus concluded that, while the lattice conductivity is not appreciably influenced by sintering time, the grain-boundary effect increases with increasing sintering.

Another set of experiments was designed to determine whether the grain-boundary conductivity shows a different dependence on P_{O_2} than does the lattice conductivity. The circles in Fig. 10 show the dc conductivity for a 1% Y_2O_3 sample at a tempera-

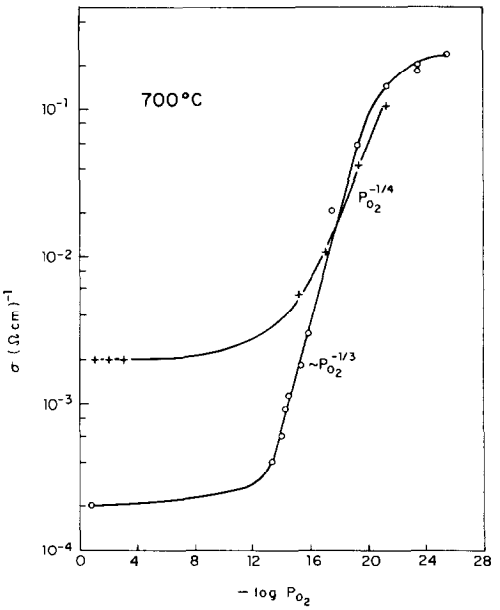

FIG. 10. Variation of dc conductivity with P_{O_2} for two samples. Circles are the grain-boundary conductivity for a 1% Y_2O_3 sample, while crosses represent lattice conductivity for a 1% CaO sample (the latter taken from Ref. (*12*)).

ture of 700°C, where the separation $\Delta \log \sigma$ between the lattice and grain-boundary conductivities is still appreciable. For each measurement, sufficient time was allowed in order to achieve equilibrium. These results for σ_{gb} show a rather strong P_{O_2} dependence ($\propto P_{O_2}^{-1/3}$ below 10^{-14} atm). While data are not available for the lattice conductivity, σ_l, of the sample sample, Fig. 10 shows data for a 1% CaO sample (*12*) for which σ_l at 700°C is close to that for the 1% Y_2O_3 sample. It is striking that the latter sample shows nothing steeper than the expected $-\frac{1}{4}$ power dependence (*12*), and also that its conductivity levels off sooner than does the grain-boundary conductivity.

Discussion

The present work shows features of the grain-boundary effect which are strikingly different from previous work on stabilized zirconia, as follows:

(1) The larger grain-boundary effects occur for low temperatures and low dopant concentrations, and the effect is almost gone at high concentrations ~15 mole% (see Figs. 5 and 8). In the case of zirconia, on the other hand, due to the need to stablize the fluorite structure, only high dopant concentrations (usually $\gtrsim$ 15%) are reported.

(2) The activation enthalpy for the grain-boundary conductivity, H_{gb}, is substantially greater than that for the lattice conductivity, H_l, especially for low dopant concentrations. In contrast, for zirconia it is observed that $H_{gb} \simeq H_l$.

(3) The effect increases with increasing sintering time, in contrast to Ref. (*7*).

In view of item (2), that $H_{gb} > H_l$, we may anticipate that, at elevated temperatures, a crossover may take place above which the grain-boundary resistance is no longer blocking the total current flow. Under these conditions, the high-temperature dc conductivity should fall on an extension of the low-temperature lattice conductivity, σ_l, rather than of the grain-boundary conductivity, σ_{gb}. In Fig. 8 this is indeed observed. Such changes in slope may account for apparent breaks in conductivity plots, as reported for example by Kudo and Obayashi (*13*), who used fixed-frequency (1 kHz) ac measurements.

The behavior reported here for doped CeO_2 seems to be in accord with that observed for doped ThO_2 by Schouler *et al.* (*14*) although, due to the lower lattice conductivity of thoria, the arcs are not as clearly separated. Nevertheless, we believe that their first arc (called Z_1Z_2) is equivalent to our grain-boundary arc 2. Indeed, they observe a steeper value of H for the low-frequency intercept than for the high-frequency intercept, and a larger separation at low Y_2O_3 concentrations. On this basis, both of the above features (1) and (2) apply as well to ThO_2 as to CeO_2.

Turning to the question of the origin of the grain-boundary effect, we run into some difficulties. On the one hand, it seems inevitable that the extra arc must be caused by a high-resistivity layer at the grain boundaries. Further, the fact that $H_{gb} > H_l$ indicates that this layer exists over the entire grain-boundary region, in contrast to the Bauerle constriction model (*2*) which was based on data for zirconia indicating that $H_{gb} = H_l$. On the other hand, the exact nature of such a layer must remain in doubt until suitable microanalytical techniques can be applied. Nevertheless, it is interesting to note that several of the present observations point to the possibility that this region may be one in which the effective dopant concentration is substantially reduced:

(a) The activation enthalpy H_{gb} seems to approach a maximum value above 2 eV as the dopant or contaminant concentration decreases (see Table III). This is consistent with the value of 2.4 eV for pure CeO_2 single crystals in the $P_{O_2}^{-1/6}$ region (*15*).

(b) The conductivity σ_{gb} increases more rapidly with decreasing P_{O_2} than does σ_l (see Fig. 10).

(c) The magnitude of the grain-boundary effect (Δ log σ) decreases and σ_{gb} itself increases with increasing dopant concentration, until σ_{gb} becomes at least equal to σ_l. This observation suggests that, although the dopant concentration in the grain-boundary region is decreased, the decrease is not sufficient for the grain-boundary resistivity to dominate the electrical behavior once the average concentration becomes high.

A possible cause of this behavior is the presence of a contaminant that reacts with, or otherwise scavenges, the dopant in the grain-boundary region. For shorter sintering times this process apparently does not have sufficient time to take place (see Fig. 9). Such a contaminant can be present in the starting material or be introduced from furnace materials during sintering. The present results also suggest that the contaminant is more effective in scavenging Y^{3+} than Ca^{2+} ions.

Finally, it is worth reemphasizing the importance of the grain-boundary effect. First, for basic studies, it is essential to be able to determine the true lattice conductivity and its dependence on concentration and temperature. In this paper, we have shown that complex impedance analysis allows a clear separation of σ_l from the other effects. A detailed report on a study of lattice conduction will be given in a forthcoming paper, a preliminary version of which has already appeared (*16*). The second importance of the effect is for applications of these electrolytes. The present results show that near 700°C one may lose as much as two orders of magnitude in conductivity as a consequence of the grain-boundary effect. For this reason it is important to know how to control or eliminate the effect. The fact that a shorter sintering treatment decreases the effect is useful, but it would be still better to eliminate the responsible contaminants, if possible.

Acknowledgments

The authors are grateful to Dr. Dong-Sil Park and Mr. John Griffith for contributing some of the measurements quoted herein, and to the U.S. Department of Energy for their support under Contract ER-78-S-02-4693.

References

1. F. J. ROHR, *in* "Solid Electrolytes" (P. Hagenmuller and W. van Gool, Eds.), Chap. 25, Academic Press, New York, 1978.
2. J. E. BAUERLE, *J. Phys. Chem. Solids* **30**, 2657 (1969).
3. J. M. HODGE, M. D. INGRAM, AND A. R. WEST, *J. Electroanal. Chem.* **74**, 125 (1976).
4. J. R. MACDONALD, *in* "Electrode Processes in Solid State Ionics" (M. Kleitz and J. Dupuy, Eds.), p. 149, Reidel, Dordtrecht, 1976.
5. N. M. BEEKMANS AND L. HEYNE, *Electrochim. Acta* **21**, 303 (1976).
6. E. SCHOULER, G. GIROUD, AND M. KLEITZ, *J. Chim. Phys.* **70**, 1309, (1973).
7. S. H. CHU AND M. A. SEITZ, *J. Solid State Chem.* **23**, 297 (1978).
8. R. W. POWERS AND S. P. MITOFF, *J. Electrochem. Soc.* **122**, 226 (1975).
9. R. W. POWERS, *in* "Superionic Conductors" (G. D. Mahan and W. L. Roth, Eds.), p. 351, Plenum, New York, 1976.
10. H. L. TULLER AND A. S. NOWICK, *J. Electrochem. Soc.* **126**, 255 (1975).
11. DA YU WANG AND A. S. NOWICK, *J. Electrochem. Soc.* **126**, 1166 (1979).
12. R. N. BLUMENTHAL, F. S. BRUGNER, AND J. E. GARNIER, *J. Electrochem. Soc.* **120**, 1230 (1973).
13. T. KUDO AND H. OBAYASHI, *J. Electrochem. Soc.* **122** 142 (1975).
14. E. SCHOULER, A. HAMMOU, AND M. KLEITZ, *Mater. Res. Bull.* **11**, 1137 (1976).
15. H. L. TULLER AND A. S. NOWICK, *J. Electrochem. Soc.* **126**, 209 (1979).
16. A. S. NOWICK, D. Y. WANG, D. S. PARK, AND J. GRIFFITH, *in* "Fast Ion Transport in Solids" (P. Vashishta *et al.*, Eds.), p. 673, North-Holland, Amsterdam (1979).